

Influences of Ca nonstoichiometry on the superconducting properties of Bi-2212 superconducting bulks

Shengnan Zhang¹ · Chengshan Li¹ · Qingbin Hao¹ · Jianqing Feng¹ · Xiaobo Ma¹ · Pingxiang Zhang¹

Received: 1 March 2015 / Accepted: 9 June 2015 / Published online: 16 June 2015
© Springer Science+Business Media New York 2015

Abstract Polycrystalline bulks of $\text{Bi}_2\text{Sr}_2\text{Ca}_x\text{Cu}_{2.0}\text{O}_{8+\delta}$ (Bi-2212) with $x = 0.90, 0.95, 1.00$ and 1.05 were fabricated by spark plasma sintering technique. The influences of Ca nonstoichiometry on the microstructures, carrier concentration, as well as the related superconducting properties were systematically investigated. XRD analyses revealed the corresponding change of lattice parameters of Bi-2212 phase with the Ca nonstoichiometry. The average particle radius in the sintered bulks underwent an obvious change with the increase of Ca content, which could be attributed to the variation of thermodynamic properties. AC susceptibility measurements exhibited the optimization of intergrain connections in $\text{Ca} = 0.95$ bulk, which lead to the optimization of both self- and in-field critical current density, J_c of this system. The optimization of microstructures also caused the enhancement of surface pinning. Based on the enhancements of both intergrain connections and flux pinning properties, an obvious improvement of critical current density was obtained with the optimal doping content of $\text{Ca} = 0.95$.

1 Introduction

Since the first discovery of $\text{Bi}_2\text{Sr}_2\text{CaCu}_2\text{O}_x$ (Bi-2212), it is considered to be one of the most promising high-temperature superconductors (HTS) due to its outstanding properties under low-temperature and high magnetic fields [1]. Meanwhile, as the only HTS so far, which can be made into

round wires with isotropic cross sections, it greatly simplifies the winding process for Rutherford cables and magnets. Therefore, it shows great potentials for the applications as insert coils in high field magnets and Rutherford cables for accelerators [2–5]. Recently, the maximum total magnetic field of 33.8 T was successfully achieved under the background field of 31.2 T with Bi-2212 insert coils [6]. And higher performances can be expected considering the defective terminal, which was heat treated in a lower temperature zone of the furnace [7]. Thus aiming at large scale applications, further improvement of the superconducting properties of Bi-2212 with simple and practical method is urgent.

There are two crucial factors which still limit the transport properties of Bi-2212 superconductors. One is the intergrain weak links due to the misalignment of grains [8–10], appearance of bubbles [11, 12] and/or grain boundaries combining with secondary phases or amorphous layers [13, 14]. The other is the intrinsic weak flux pinning, which can be attributed to its layered lattice structures with the large anisotropic parameter $\gamma > 50$ [15]. Therefore, fabrication of Bi-2212 superconductors with higher textural structure, cleaner grain boundaries and stronger flux pinning properties can contribute to the enhancement of current carrying capacity of Bi-2212 for practical applications. Based on previous studies, tuning the chemical composition in Bi-2212 phase may provide various effects on the optimization of HTS materials by tuning the lattice structure, microstructures, thermodynamic behaviors, and electric/magnetic properties. Pb doping at Bi site of Bi-2212 is considered to be the most successful example [16, 17]. The crystal structure of Bi-2212 is considered to be orthorhombic, with the lattice parameter $a \approx b \approx 5.41 \text{ \AA}$, and $c \approx 30.84 \text{ \AA}$. The large difference between c and a (b) is the structural cause of the large anisotropic

✉ Shengnan Zhang
snzhang@c-nin.com

¹ Superconducting Materials Research Center, Northwest Institute for Nonferrous Metal Research, Xi'an 710016, China

parameter. The introduction of Pb can decrease the lattice parameter c of Bi-2212, which not only reduces its anisotropic parameter, but also introduces effective flux pinning centers to enhance the in-field current capacity. Rare earth (RE) elements doping on the Sr/Ca site of Bi-2212 are also studied [18–22]. RE ions, such as Ho^{3+} , La^{3+} and Eu^{3+} can work as effective pinning centers to enhance the flux pinning properties, thus lead to an obvious increase of critical current density. Besides, B_2O_3 doping [23] results in the faster growth and better alignment of the Bi-2223 grains by tuning its thermodynamic properties, which also improved the critical current density.

On the other hand, Majewski et al. [24] reported that the Ca/Sr rich composition could lead to the increase of critical current density of Bi-2212 bulks due to the enhancement of flux pinning properties. Thus the introduction of nonstoichiometry can also be recognized as a simple way to optimize the superconducting properties of Bi-2212. In this study, Ca nonstoichiometry is introduced into Bi-2212 bulks. The influences of different Ca content on the microstructures, electric and superconducting properties including weak link behavior and flux pinning mechanism are systematically investigated.

2 Experimental details

$\text{Bi}_2\text{Sr}_2\text{Ca}_x\text{Cu}_{2.0}\text{O}_{8+\delta}$ ($x = 0.90, 0.95, 1.00$, and 1.05) precursor powders were prepared by modified co-precipitation process with the starting materials of Bi_2O_3 , SrCO_3 , CaCO_3 , and CuO (>99.9 %). Single phased Bi-2212 precursor powders with different Ca content were obtained after a series of calcination processes in air at $800\text{ }^\circ\text{C}/12\text{ h}$, $820\text{ }^\circ\text{C}/20\text{ h}$, and $850\text{ }^\circ\text{C}/20\text{ h}$ with intermediate grinding. The precursor powders were then densely packed in a graphite die and pressed into pellets with the diameter of $\phi 12.7\text{ mm}$, and thickness of 1.5 mm by spark plasma sintering technique, with the sintering temperature of $780\text{ }^\circ\text{C}$, and sintering time of 5 min . The post annealing process was taken under $500\text{ }^\circ\text{C}$ for 24 h in oxygen atmosphere, in order to optimize the oxygen content of superconducting phase.

The density of bulk was measured using standard Archimedes method after annealing. Polycrystalline X-ray diffraction (XRD) patterns on both powders and bulks were taken on an X-ray diffraction (XRD, Bruker D8 Advance) with $\text{Cu-K}\alpha$ radiation ($\lambda = 0.1542\text{ nm}$). The texture degrees of $(00l)$ peaks were mostly used to just the quality of texture structures, which were calculated as following,

$$F_{00l} = \frac{\sum I_{00l}}{\sum I} \times 100\% \quad (1)$$

where I_{00l} represents for the $(00l)$ peak intensity of Bi-2212 phase, $\sum I$ is the total diffraction intensity of the pattern.

The chemical compositions of precursor powders were measured by inductive coupled plasma atomic emission spectrometry (ICP-AES) with IRIS[®] Advantage ICP-AES. The scanning electron microscopy (SEM) images were obtained with JEOL JSM-6700F. The thermopower values were measured on ZEM-2 within the temperature range of room temperature to $150\text{ }^\circ\text{C}$ with the temperature difference of $10\text{ }^\circ\text{C}$. Four thermopower values were taken at one temperature to obtain the average value. Pellets were cut into cubes with the surface area of $\sim 2 \times 2\text{ mm}^2$ and same thickness (1.5 mm) for the magnetic properties measurement. AC susceptibility was measured by the Superconducting Quantum Interference Device (SQUID, MPMS-XL-7) with the AC magnetic field of $0.01, 0.1, 0.5, 1.0$ and 1.5 Oe and frequency of 333 Hz . Then, the same sample was used for the magnetic susceptibility measurement by SQUID under the temperature of 20 K and background field of $0\text{--}2\text{ T}$. The sample was placed in the field parallel to the SPS pressing direction. After that, BEAN model [25] was adopted for the calculation of the critical current density (J_c) as shown below,

$$J_c = \frac{20\Delta M}{b(1 - b/3a)} (b < a) \quad (2)$$

where a and b are the length and the width of the bulk respectively ($a \approx 2\text{ mm}$, $b \approx 2\text{ mm}$), which are both perpendicular to the applied magnetic field, and ΔM is the difference between M^+ (magnetization values under increasing field) and M^- (magnetization values under decreasing field) at same magnetic field.

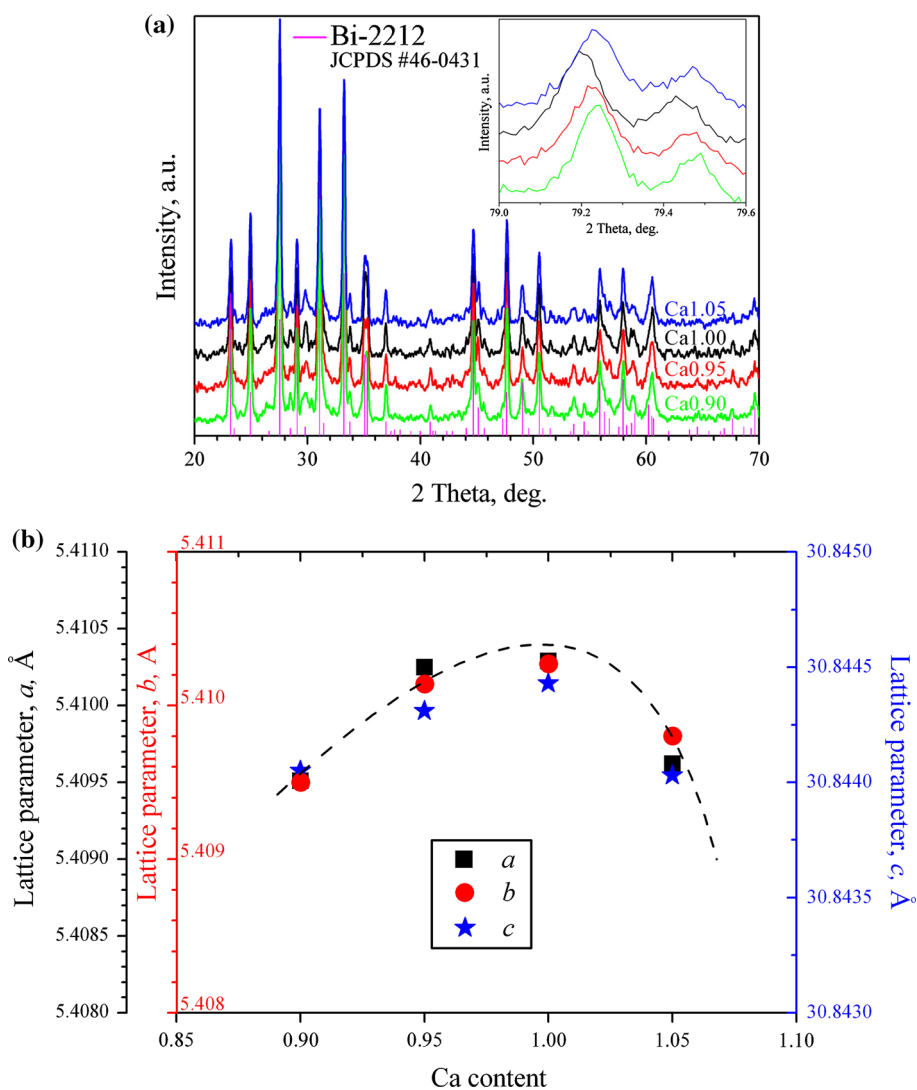
3 Results and discussion

Ca content in the precursor powders are measured by ICP and listed in Table 1 after normalizing the Ca content to Bi content of 2.1. The Ca contents in obtained precursor powders are consistent with the nominal composition. The diffraction patterns of precursor powders are plotted in Fig. 1a. The major phase in precursor powders after calcination can be indexed into Bi-2212 with orthorhombic structure. Besides as shown in the inset of Fig. 1a, the diffraction peaks of Bi-2212 phases shift with the increasing Ca content, which implies the change of lattice parameters. With the refinement of XRD patterns, lattice parameters a , b and c are estimated and plotted in Fig. 1b. The a and b values of each sample are similar, suggesting the near tetragonal lattice structure. With the increasing Ca content, the lattice parameters increase first, and then decrease. The maximum lattice volume is obtained at Ca stoichiometric sample. The decrease of lattice parameters from $\text{Ca} = 1.00$ to 0.90 can be attributed to the shrink of lattice with the absence of Ca ions. On the other hand, with

Table 1 Physical properties of Bi-2212 with Ca content of $x = 0.90, 0.95, 1.00,$ and 1.05

Nominal Ca content (x)	0.90	0.95	1.00	1.05
Ca content by ICP normalized to Sr = 2.0	0.86 (3)	0.94 (4)	0.98 (2)	1.04 (2)
Texture degree (%)	62.6	64.1	60.1	62.4
Density (g cm^{-3})	5.79 (1)	5.77 (8)	5.76 (0)	5.72 (1)
Critical temperature [T_c^{onset} (K)]	82	85	86	87
Carrier concentration, per Cu ion	0.195	0.178	0.183	0.190
Peak temperature [T_p , K (@ $H_{ac} = 0.5$ Oe)]	62	69	74	50
Average radius (μm)	3.9 (1)	6.0 (5)	4.3 (2)	3.8 (8)
J_c (@20 K, 0 T) (A cm^{-2})	119.5	205.4	127.8	80.3

Numbers in parenthesis are statistical standard deviations of the last significant digit

Fig. 1 a Powder diffraction patterns of Bi-2212 precursor powders with Ca = 0.90, 0.95, 1.00, and 1.05. Two diffraction peaks were zoomed in the *inset* from 79° to 79.6° . **b** Lattice parameters a , b , and c change with Ca content, with the *dashed line* guide to eyes

the increase of Ca content over stoichiometric value to 1.05, the decrease of lattice parameters can be related to the introduction of excess oxygen incorporated between the Bi–O double layers to balance the electrons introduced by excess Ca^{2+} [26–28], which reduces the net positive charge

and hence the repulsion force between the Bi–O layers, thus causes the slab sequence SrO–BiO–BiO–SrO to shrink [29].

Spark plasma sintering (SPS) process is adopted for the sintering of Bi-2212 bulks with different Ca content. The

densities of these bulks are measured and listed in Table 1. The density variation of ~1 % is within the error range of Archimedes method. Therefore, no obvious change of density with Ca content is observed. Since SPS process is effective for the fabrication of high density bulks, all the density of Bi-2212 bulks are higher than >85 % of theoretical density. The X-ray diffraction patterns of bulks after sintering and annealing are plotted in Fig. 2. After the heat

treatment processes, Bi-2212 is still the major phase in all these bulks. While as marked in Fig. 2, in the bulk with lower Ca content, the diffraction peaks of Bi₂Sr₂CuO₆ can be observed. This is consistent with the phase diagram studies by Majewski et al. [30, 31]. (00l) texture is obtained in the bulks after SPS. After the calculation of texture degree with Eq. 1 as listed in Table 1, the maximum texture degree of 64.1 % is obtained in the Bi-2212 bulk with Ca content of 0.95. Based on our previous study, it is assumed that the change of textural structures can be attributed to the thermodynamic properties change, which dominants both the phase evolution process and the growing process of grains [32].

As shown in Fig. 3a–d, the SEM images of the fractured surface of the *x* = 0.90–1.05 bulks are obtained. No obvious pores can be observed, which indicates the dense structure by SPS method. Texture structures can be observed in all these images, especially in Ca = 0.95 and 1.00 bulks, with the surface of plate-like grains perpendicular to the pressing direction as marked in each image. With the increase of Ca doping content, the texture orientation is enhanced first then decreased. On the other hand, by analyzing these images, the average grain radius of these bulks is estimated and listed in Table 1. Obvious increase of grain radius is observed with the proper Ca content of 0.95–1.00. And the maximum average grain radius of 6.0 μm is obtained with the Ca content of

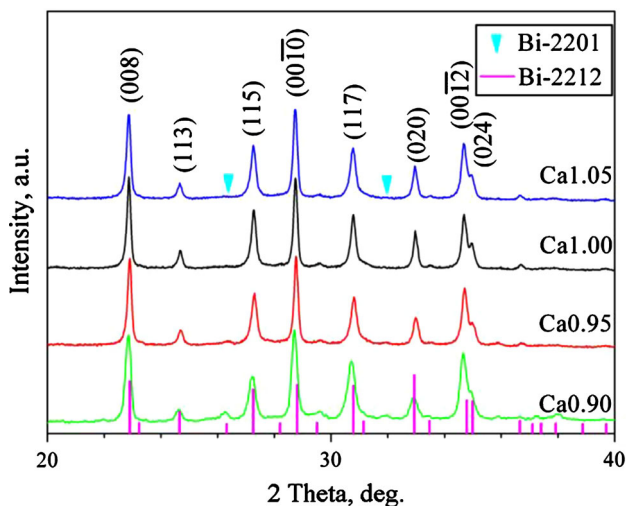
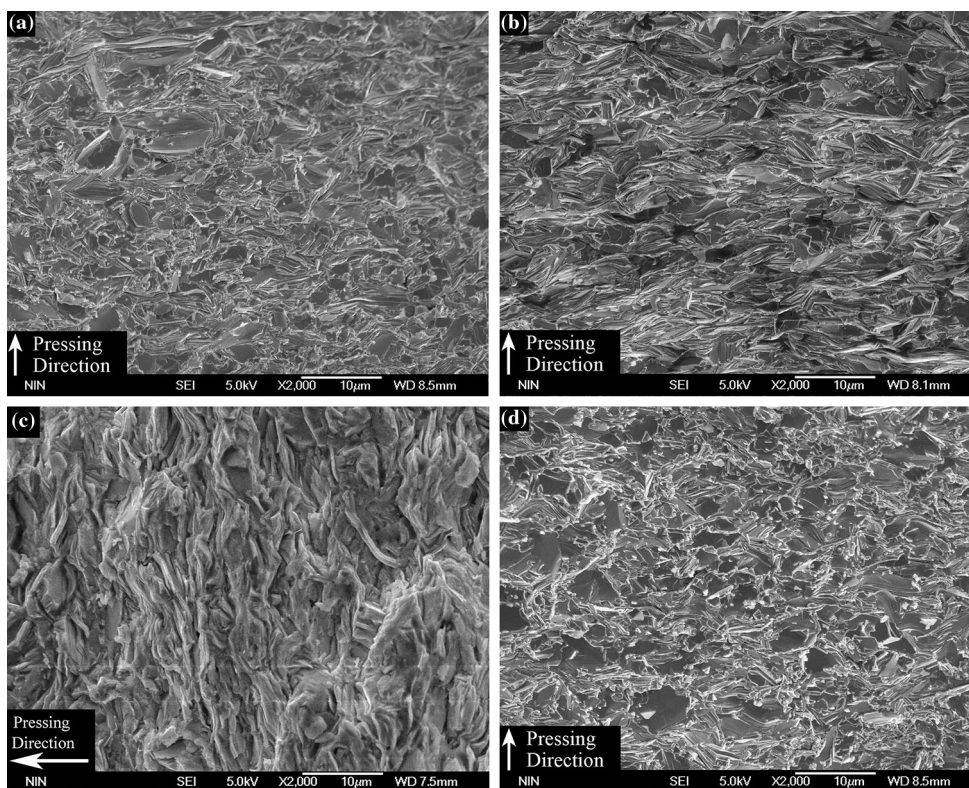


Fig. 2 XRD patterns of Bi-2212 bulks with different Ca content of *x* = 0.90, 0.95, 1.00 and 1.05

Fig. 3 Typical SEM images of fractured surface of Bi-2212 bulks with different Ca content of **a** *x* = 0.90, **b** *x* = 0.95, **c** *x* = 1.00 and **d** *x* = 1.05. The pressing direction of bulks was marked in each image correspondingly



$x = 0.95$. It can be deduced that due to the change of thermodynamic properties, more melts appear during the sintering process, which can obviously improve the growth of Bi-2212 grains. However, with the further increase of Ca content to $x = 1.05$, nuclear rate increases which then lead to the decrease of particle size.

One important influence of the Ca content change in Bi-2212 matrix is on the carrier concentrations. In cuprates high temperature superconductors, the main carriers are holes [39]. According to the previous report by Tallon et al. [33], for small hole concentration per Cu ion, p , ($p < 0.2$), the following equation can be used to estimate the hole concentration values by the room temperature thermopowers:

$$S = \frac{k_B}{e} \left(\ln \frac{1-p}{2p} - \ln 2 \right) \quad (3)$$

where, k_B and e are the Boltzmann constant and electron charge, respectively, S is thermopower with the unit of μVK^{-1} , the extra $\ln 2$ term comes from the orbital degrees of freedom (assuming two fold orbital degeneracy). This equation is derived using a single-band Hubbard model with the assumption that the bandwidth is much less than $k_B T$. Therefore, by measuring the thermopower values, it is possible to study the carrier concentration change and electric transport behavior of normal state qualitatively.

The thermopower values are measured before and after the annealing process in oxygen and the thermopower values at 25 °C are adopted for the calculation of carrier concentration. As shown in Fig. 4a, the thermopower values decrease obviously after annealing, which contributes to the great increase of carrier concentration as shown in Fig. 4b. It is because the oxygen content of these bulks increases after oxygen annealing, which leads to the introduction of more holes in Bi-2212. Meanwhile, with the increasing Ca content, the carrier concentrations before and after annealing are both decrease first then increase. This change suggests that the electronic structure of Bi-2212, especially on the $[\text{Cu}-\text{O}_2]$ layers can be tuned with the change of Ca content. First, with the Ca content increase from 0.90 to 0.95, more electrons are introduced, which neutralize holes and lead to the decrease of carrier concentration. Then with the further increase of Ca content, oxygen content also increases in order to achieve a new equilibrium state as discussed above, which causes the formation of more holes. Thus the carrier concentration increases. And the change of carrier concentration is crucial for the superconducting properties of Bi-2212 [34].

The AC susceptibility is widely used as a nondestructive method for the determination and characterization of the intergrain connections in the polycrystalline high temperature superconductors, as well as the flux pinning properties [35–38]. The temperature dependencies of the real, χ' ,

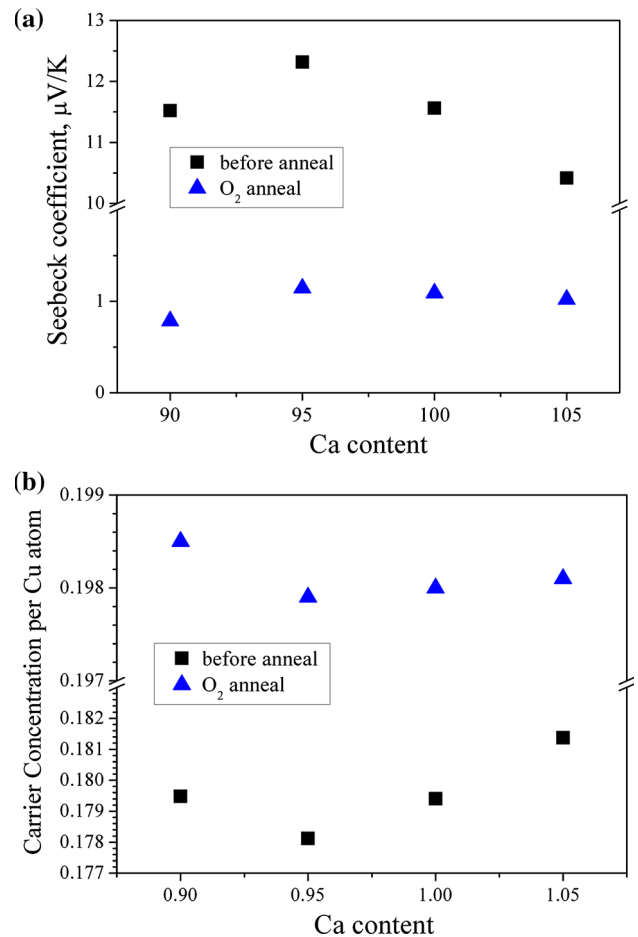


Fig. 4 **a** Thermopower values and **b** carrier concentrations of Bi-2212 bulks as a function of Ca content ($x = 0.90, 0.95, 1.00,$ and 1.05)

and imaginary, χ'' , components of AC susceptibility for the Bi-2212 bulks with Ca content of $x = 0.90, 0.95, 1.00,$ and 1.05 are measured in AC field of 0.5 Oe with the frequency of 333 Hz and plotted in Fig. 5a. It is observed that for all these samples, the real components of AC susceptibility, χ' , as shown in Fig. 5b show two drops with the decreasing temperature. The first drop is due to the transition within grains at T_c , which can be recognized as the critical temperature of these bulks. By zooming in the transition part as shown in the inset of Fig. 5b, the T_c values are obtained as listed in Table 1. The critical temperature increases with Ca content from 82–87 K, with the maximum T_c of 87 K obtained with Ca = 1.05. The carrier concentration dependence of critical temperature is plotted in Fig. 5c. It is noticed that the Bi-2212 bulks with Ca = 0.90 is in the over-doping region. And with the increase of Ca content, the bulks are tuned to the under-doping region with the decrease of carrier concentration. Then the sample enters into the optimal doping region with the Ca content of 1.05.

The second drop is induced by macroscopic shielding currents through grains and weak links. In the temperature

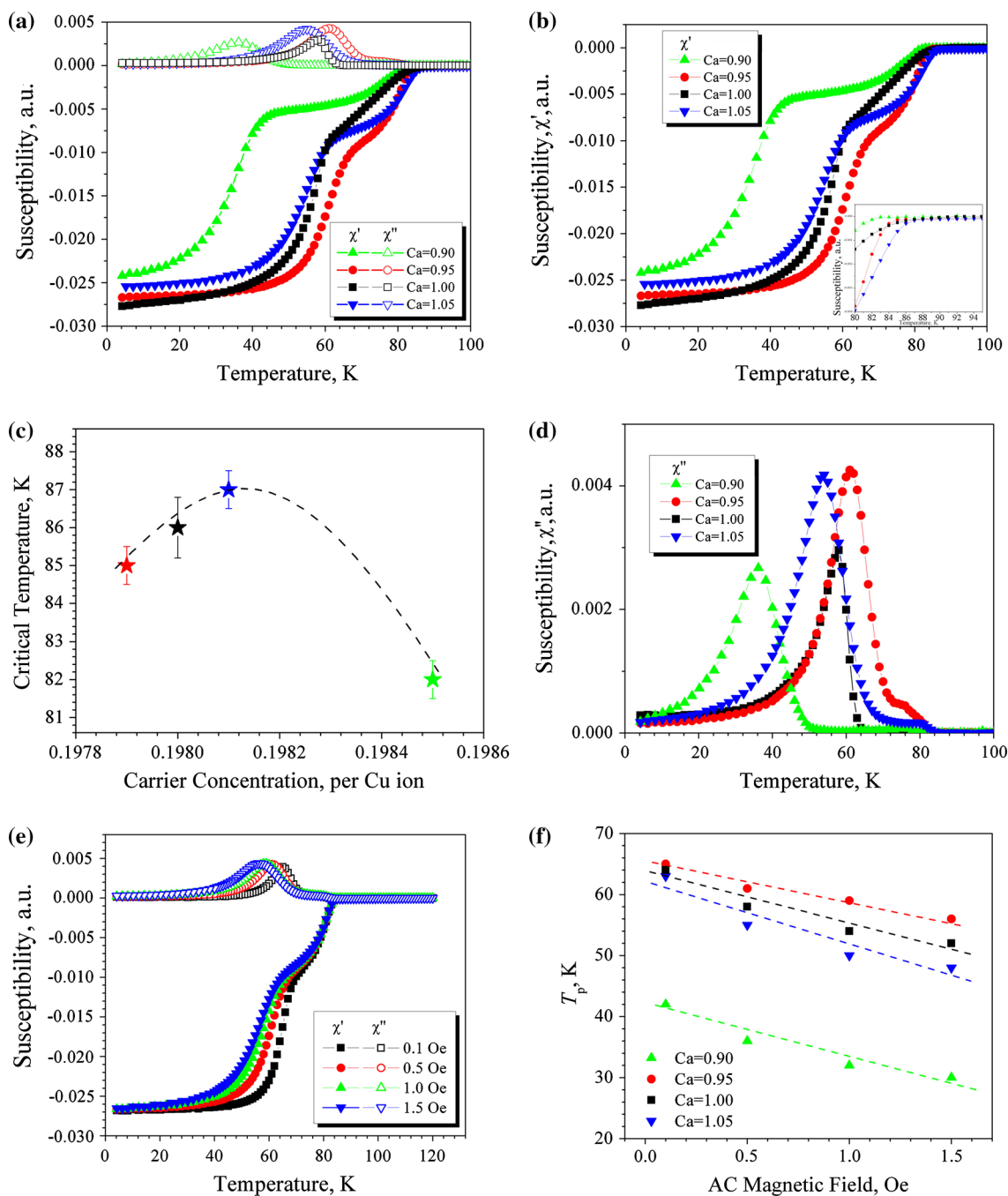


Fig. 5 **a** Temperature dependence of the AC susceptibility for Bi-2212 bulks with Ca content of $x = 0.90, 0.95, 1.00,$ and 1.05 in the AC field amplitude of 0.5 Oe at the frequency of 333 Hz; The real χ' and imaginary χ'' components were plotted in **(b)** and **(d)** separately, and the transition areas of the real component were zoomed in **(b)**. The critical temperature values were plotted in **(c)** as a function of

carrier concentration; The temperature dependence of the AC susceptibility measured in different AC field, $H_{ac} = 0.1, 0.5, 1.0,$ and 1.5 Oe at the frequency of 333 Hz for Bi-2212 bulks with Ca content of $x = 0.95$ is plotted in **(e)**; **f** the AC field dependence of peak temperature, T_p , with the linear fitting shown as *dashed lines*

range between the first and second drop, the superconducting grains are decoupled by the penetration of the applied field through the grain boundary. However, the weak links can carry a supercurrent if the temperature is below the point at which coupling energy is equal to

thermal energy. The second drop in χ' can thus give an information on the character of weak links, thus to analyze the intergrain connections. Correspondingly, on each of the imaginary component curve, χ'' , a peak appears, which is the measure of dissipation in the sample. Therefore, by

examining the change of peak temperature, T_p , on the χ'' curve, the character of weak link in the superconducting materials can be discussed. As shown in Fig. 5d, the T_p values increase with Ca content from 0.90 to 0.95 then decrease. This result suggests that the intergranular coupling between grains in Bi-2212 sample is improved by proper amount of Ca nonstoichiometry and better inter-grain connections are achieved.

The flux pinning properties of high temperature superconducting bulks are also discussed based on the analyses of the χ'' -T behavior under different AC magnetic field. The temperature dependence of AC susceptibility of Ca = 0.95 bulk under different AC fields, H_{ac} , are plotted in Fig. 5e as an example. With the increase of H_{ac} , the peak of χ'' shifts towards lower temperature and broadened. Thus the dependences of T_p on H_{ac} of the bulks with Ca content of 0.90 ~ 1.05 are plotted in Fig. 5f. It can be observed that the T_p values of Ca = 0.95 bulk are higher than those of stoichiometric bulk within the entire applied AC field range. By fitting the T_p - H_{ac} curves with the linear dependence from the Müller model [39], the intra-granular pinning force can be estimated with Eq. 4.

$$T_p = T_c \left(1 - \left(\frac{\mu_0}{8R_g \alpha_g(0)} \right)^{1/2} H_{ac} \right) \quad (4)$$

where, the values of T_c and T_p are taken from the AC susceptibility measurement, R_g is the average grain radius, which is measured on the SEM images as discussed above, $\alpha_g(0)$ is the intra-granular pinning force density for Abrikosov vortices. In order to compare the pinning force density of these samples, we assume the $\alpha_g(0)$ of Ca stoichiometric sample to be $\alpha'_g(0)$, and the obtained $\alpha_g(0)$ of $x = 0.90, 0.95$ and 1.05 samples are $1.21\alpha'_g(0)$, $1.44\alpha'_g(0)$ and $0.81\alpha'_g(0)$, respectively. These results indicate that proper amount of Ca nonstoichiometry can effectively enhance the intra-granular pinning force density for Abrikosov vortices.

The critical current densities of Bi-2212 bulks with different Ca content are calculated based on the magnetization measurement within the magnetic field of 0–2 T at 20 K. As shown in Fig. 6a, over the entire measured magnetic field range, the critical current densities of the Ca = 0.95 bulk are higher than that of the stoichiometric bulk. The self-field J_c increases obviously from 128 to 205 A cm⁻² which is about 60 % increase. This increase of J_c at self field can be attributed to the enhancement of both texture structure and intergrain connections as discussed above.

The pinning force densities of Bi-2212 bulks with different Ca content are calculated with the equation $F_p = J_c \times B$. The pinning force density F_p as a function of magnetic fields B is plotted in Fig. 6b. Obvious

enhancement of flux pinning properties is observed for Ca = 0.95 bulk, which contributes to the increase of in-field J_c . Meanwhile, as shown in the inset, the flux pinning mechanism change can be investigated by fitting the scale plots of normalized pinning force density ($f = F_p/F_{pmax}$) as a function of reduced magnetic fields ($b = B/B_{irr}$) with the Dew-Hughes equation [40]:

$$F_p = A(B/B_{irr})^p (1 - B/B_{irr})^q \quad (5)$$

where A is a numerical parameter independent of the applied field, B_{irr} is the irreversible field, p and q are parameters describing the actual pinning mechanism. The fitting parameters for different samples are given in Table 2. All the samples exhibit similar p and q values of $p \sim 0.5$ and $q \sim 2$, which implies the surface pinning is dominant pinning mechanism in these bulks [21]. Therefore, grain boundaries is important for not only the inter-grain connections but also the flux pinning properties in these bulks. The Ca = 0.95 bulk exhibit larger grain radius, which based on our previous studies implies the enhanced crystallization behavior of Bi-2212 phase [41]. Thus the grain boundaries are also well crystallized and can work as effective pinning centers. Although the intra-granular pinning force density for Abrikosov vortices of the Ca = 0.90 sample is higher than that of stoichiometric bulk, the number of effective surface pinning centers decreases considering the small grain size which dominates the overall flux pinning properties. While for the Ca = 1.05 bulk, the p value increases to 0.70, suggesting the weakening of surface pinning and enhancement of point pinning in this sample. It indicates that the introduction of excess Ca ions can lead to the formation of point defects in Bi-2212 matrix, which can work as effective point pinning centers.

4 Conclusions

Bi-2212 superconducting bulks with different Ca content were fabricated with SPS method. The influences of Ca nonstoichiometry on the lattice parameter, microstructure, carrier concentration, and related superconducting properties were investigated. The Ca nonstoichiometry can not only lead to the formation of point defects as Ca vacancy in Bi-2212 matrix, but also cause the change of oxygen content in order to achieve a new equilibrium state. Therefore both the lattice parameters and the carrier concentrations changed correspondingly. The maximum critical temperature of 87 K was achieved with Ca content of 1.05 when the carrier concentration was in the optimal doping region. The microstructure change was crucial for not only the intergrain connections but also the flux pinning properties, considering the dominant flux pinning

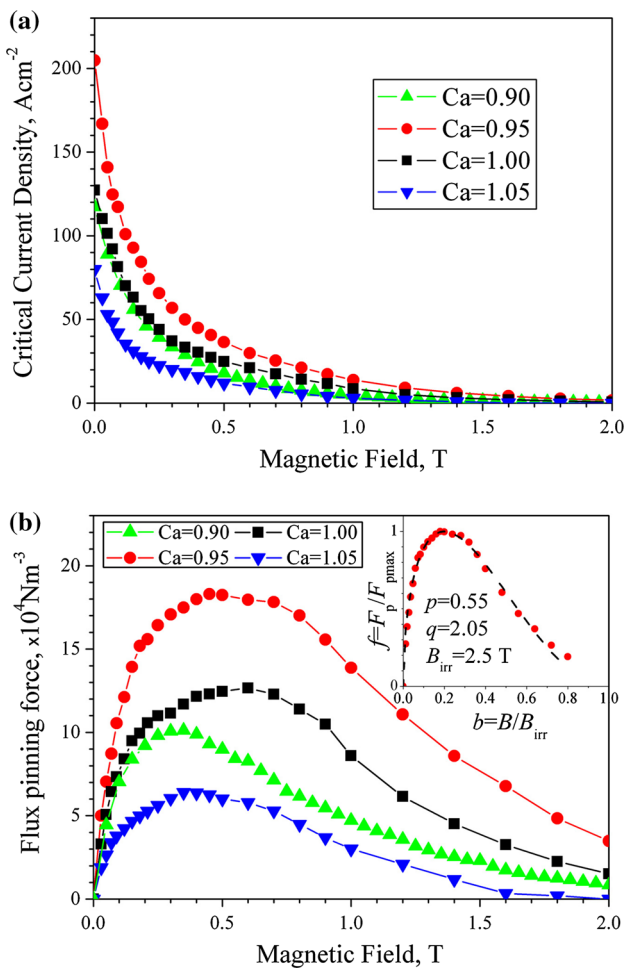


Fig. 6 **a** Magnetic field dependence of critical current density and **b** Reduced Flux pinning force as a function of reduced magnetic field of Bi-2212 bulks with different Ca content in the magnetic field of 0–2 T at 20 K. The Dew-Hughes fitting of f - b curve of Ca = 0.95 bulk is plotted in the *inset* with the *red dots* for experimental data and *black line* for fitting curve (Color figure online)

Table 2 Values of pinning parameters for Bi-2212 bulks with different Ca content of $x = 0.90$ – 1.05 obtained with Dew-Hughes model

x value	0.90	0.95	1.00	1.05
p	0.55	0.55	0.59	0.70
q	2.75	2.09	2.16	2.61
B_{irr} (T)	2.1	2.5	2.3	1.9
A ($\times 10^6$ Nm $^{-3}$)	4.48	7.07	5.29	3.53

mechanism of these bulks were all surface pinning. Therefore, obvious improvements of critical current density were obtained with Ca = 0.95 due to both the improvement of intergrain connections and the enhancement of flux pinning properties.

Acknowledgments This research was financially supported by National “973” Project, under Contract No. 2011CBA00104, National Natural Science Foundation of China under Contract No. 51472206, the international scientific and technological cooperation projects of China No. S2010GR0518, the national ITER Program of China No. 2013GB110001, and the Program for Innovative Research Team in Shaanxi Province No. 2013KCT-07.

Conflict of interest The authors declared that they have no conflicts of interest to this work.

References

- H. Miao, K.R. Marken, M. Meinesz, B. Czabaj, S. Hong, I.E.E.E. Trans. Appl. Supercond. **15**, 2554–2557 (2005)
- N. Tomita, M. Arai, E. Yanagisawa, T. Morimoto, H. Fujii, H. Kitaguchi, H. Kumakura, K. Inoue, K. Togano, H. Maeda, K. Nomura, Appl. Phys. Lett. **65**, 898–900 (2009)
- H.M. Weijers, U.P. Trociewitz, W.D. Markiewicz, J. Jiang, D. Myers, E.E. Hellstrom, A. Xu, J. Jaroszynski, P. Noyes, Y. Viouchkov, D.C. Larbalestier, I.E.E.E. Trans. Appl. Supercond. **20**, 576–582 (2010)
- T. Kiyoshi, A. Sato, H. Wada, S. Hatashi, M. Shimada, Y. Kawate, I.E.E.E. Trans. Appl. Supercond. **10**, 472–477 (1999)
- M. Dalban-Canassy, D.A. Myers, U.P. Trociewitz, J. Jiang, E.E. Hellstrom, Y. Viouchkov, D.C. Larbalestier, Supercond. Sci. Technol. **25**, 115015 (2012)
- P. Chen, U.P. Trociewitz, M. Dalban-Canassy, J. Jiang, E.E. Hellstrom, D.C. Larbalestier, Supercond. Sci. Technol. **26**, 075009 (2013)
- D.C. Larbalestier, J. Jiang, U.P. Trociewitz, F. Kametani, C. Scheuerlein, M. Dalban-Canassy, M. Matras, P. Chen, N.C. Craig, P.J. Lee, E.E. Hellstrom, Nat. Mater. **13**, 375–381 (2014)
- L.N. Bulaevskii, L.L. Daemen, M.P. Maley, J.Y. Coulter, Phys. Rev. B **48**, 13798 (1993)
- D. Buhl, T. Lang, L.J. Gauckler, Appl. Supercond. **4**, 299–317 (1997)
- S. Stassen, A. Vanderschueren, R. Cloots, A. Rulmont, M. Ausloos, J. Cryst. Growth **166**, 281–285 (1996)
- J.Y. Jiang, H.P. Miao, Y.B. Huang, S. Hong, J.A. Parrell, C. Scheuerlein, M.D. Michiel, A.K. Ghosh, U.P. Trociewitz, E.E. Hellstrom, D.C. Larbalestier, IEEE Trans. Appl. Supercond. **23**, 6400206 (2013)
- F. Kametani, E.G. Lee, T. Shen, P.J. Lee, J. Jiang, E.E. Hellstrom, D.C. Larbalestier, Supercond. Sci. Technol. **27**, 055004 (2014)
- C.J. Eastell, B.M. Henry, C.G. Morgan, C.R.M. Grovenor, M.J. Goringe, IEEE Trans. Appl. Supercond. **7**, 2083 (1997)
- Y.N. Tsay, Q. Li, Y. Zhu, M. Suenaga, K. Shibusaki, I. Shigaki, R. Ogawa, IEEE Trans. Appl. Supercond. **9**, 1662 (1999)
- Y. Nakayama, T. Motohashi, K. Otzchi, J. Shimoyama, K. Kitazawa, K. Kishio, Phys. Rev. B **62**, 1452–1456 (2000)
- R. Gladyshevskii, N. Musolino, R. Flukiger, Phys. Rev. B **70**, 184522 (2004)
- H. Fujii, Y. Hishinuma, H. Kitaguchi, H. Kumakura, K. Togano, Physica C **331**, 79–84 (2000)
- S. Dalela, B. Dalela, D. Neena, P.A. Alvi, Physica C **471**, 137–142 (2011)
- S. Bal, M. Dogruer, G. Yildirim, A. Varilci, C. Terzioglu, Y. Zalaoglu, J. Supercond. Nov. Magn. **25**, 847–856 (2011)
- S. Vinu, P.M. Sarun, A. Biju, R. Shabna, P. Guruswamy, U. Syamaprasad, Supercond. Sci. Technol. **21**, 045001 (2008)
- S. Vinu, P.M. Sarun, R. Shabna, P.M. Aswathy, J.B. Anooja, U. Syamaprasad, Phys. B **405**, 4355–4359 (2010)

22. S. Vinu, P.M. Sarun, R. Shabna, U. Syamaprasad, J. Am. Ceram. Soc. **94**, 1634–1638 (2011)
23. H. Sasakura, Y. Akagi, S. Tsukui, M. Adachi, J. Supercond. Nov. Magn. **23**, 535–538 (2010)
24. P. Majewski, S. Elschner, F. Aldinger, J. Electron. Mater. **24**, 1937–1941 (1995)
25. C.P. Bean, Phys. Rev. Lett. **8**, 250–253 (1962)
26. P. Majewski, B. Hettich, N. Ruffer, F. Aldinger, J. Electron. Mater. **22**, 1259–1262 (1993)
27. P. Majewski, H.L. Su, M. Quilitz, J. Mater. Sci. **32**, 5137–5141 (1997)
28. S. Vinu, P.M. Sarun, R. Shabna, U. Syamaprasad, J. Appl. Phys. **106**, 063920 (2009)
29. J. Kumar, P.K. Ahluwalia, H. Kisha, V.P.S. Awana, J. Supercond. Nov. Magn. **23**, 493–499 (2010)
30. P. Majewski, B. Hettich, K. Schulze, Physica C **185–189**, 469–470 (1991)
31. P. Majewski, H.L. Su, B. Hettich, Adv. Mater. **4**, 508–511 (1992)
32. S.N. Zhang, C.S. Li, T.N. Lu, Q.B. Hao, P.X. Zhang, Supercond. Sci. Technol. **28**, 045014 (2015)
33. J.L. Tallon, J.R. Cooper, P.S.I.P.N.D. Silva, G.V.M. Williams, J.W. Loram, Phys. Rev. Lett. **75**, 4114–4117 (1995)
34. C. Nguyen-Van-Huong, C. Hinnen, J.M. Siffre, J. Mater. Sci. **32**, 1725–1731 (1997)
35. H. Salamati, P. Kameli, Physica C **403**, 60–66 (2004)
36. I.H. Gul, F. Amin, A.Z. Abbasi, M. Anis-ur-Rehman, A. Maqsood, Physica C **449**, 139–147 (2006)
37. V. Mihalache, I.G. Deac, A.V. Pop, L. Miu, Curr. Appl. Phys. **11**, 1010–1014 (2011)
38. P. Kameli, H. Salamati, M. Eslami, Solid State Commun. **137**, 30–35 (2006)
39. K.-H. Muller, Physica C **159**, 717–726 (1989)
40. R.G. Hamshire, M.T. Taylor, J. Phys. F **2**, 89 (1972)
41. S.N. Zhang, C.S. Li, Q.B. Hao, J.Q. Feng, T.N. Lu, P.X. Zhang, J. Supercond. Nov. Magn. (2015). doi:[10.1007/s10948-015-2981-1](https://doi.org/10.1007/s10948-015-2981-1)